IL NUOVO CIMENTO **40 C** (2017) 98
DOI 10.1393/ncc/i2017-17098-1

COMMUNICATIONS: SIF Congress 2016

Investigation on 3D dose distribution in digital breast tomosynthesis

M. MASI
Dipartimento di Fisica "Ettore Pancini", Università di Napoli Federico II - Napoli, Italy

received 12 February 2017

Summary. — Monte Carlo calculations for dosimetry in digital breast tomosynthesis (DBT) require experimental validations. We measured the 3D dose distribution in a breast phantom in a DBT scan, using XR-QA2 radiochromic films. We positioned film pieces at the entrance surface, at the bottom surface and at four depths between adjacent slabs in the 5-slabs, 5-cm-thick phantom simulating a compressed breast with 50% glandular fraction. We irradiated the phantom at 40 kV (half value layer 1.1 mm Al) for three angular tilting of the beam central axis ($\pm 25^\circ$ and 0° normal incidence). We determined the transverse and longitudinal distributions of the average dose in the phantom (in terms of air kerma normalized to the entrance air kerma), showing the angular dependence of the depth-resolved 3D dose distributions. In transverse planes the maximum dose variations were between 5.0% and 14.8% for normal incidence, and by 8.6% from the central to the tilted view. In the direction of the beam axis, the dose decreases up to about 71% from the entrance to the exit value. The extimated backscatter fraction was between 3% and 8%.

1. – Introduction

Breast cancer may affect one in eight women during their lifetime [1]. Mammography is currently the gold standard method used to detect breast cancer in the early and asymptomatic phase. Digital mammography is a two-dimensional (2D) X-ray imaging method which produces tissue superimposition in the projected image. In order to overcome the intrinsic limitation of tissue overlap in 2D mammography (which can hinder the detection of massive lesions), a new imaging technique, digital breast tomosynthesis (DBT), has been developed: it received regulatory approval in USA and was then introduced into clinical routine in 2011. DBT is a three-dimensional (3D) X-ray imaging technique typically adopted for producing sectional views of the breast anatomy in planes transverse to the beam axis, via acquisition of a sequence of cranio-caudal or mediolateral oblique planar views of the compressed breast at several viewing angles in a range across the direction θ between the central ray of the X-ray beam and the entrance surface of the compressed breast [2]. The few commercial devices available adopt an

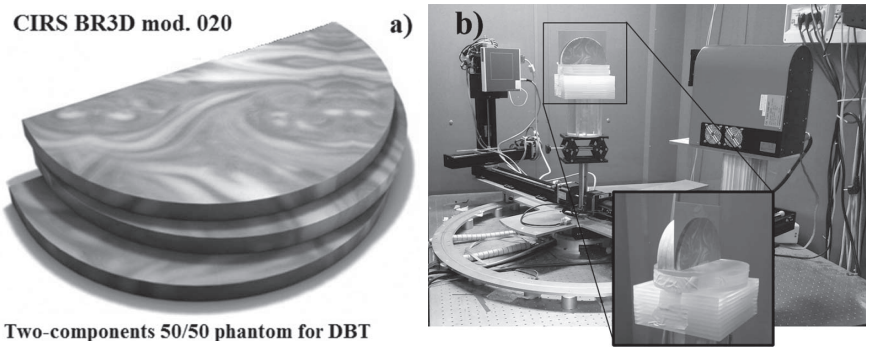

Fig. 1. – (a) Composite breast phantom. (b) Photo of the experimental setup showing the microfocus X-ray tube (foreground) and the breast phantom with radiochromic films inserted between slabs (center background). The X-ray tube can rotate around a vertical axis, simulating a DBT scan. The insert shows a magnified view of the phantom.

angular range between $\pm 5.5\,^\circ$ and $\pm 25\,^\circ$ and the number of projections acquired during the angular stepping of the X-ray tube can vary from 9 to 25 [3], in dependence of the specific DBT commercial unit. The basic components of a DBT device are: the rotating X-ray rube, the compression plate, the support plate, and the digital detector. The X-ray tube rotates around an horizontal axis in a plane around the compressed breast, and it acquires a projection transmission image of the compressed breast at each viewing angle. Sectional views of the breast are produced by off-line image reconstruction, *e.g.*, with a filtered back-projection algorithm as used in conventional computed tomography scans.

As in any diagnostic and therapeutic procedure, benefits are accompanied by risks. Mammography or tomosynthesis exposes women to a low dose of ionizing radiation, depositing energy in the radiosensitive glandular breast tissue. Hence there is a low, though not considered to be negligible, risk of radiation-induced cancer, which can be calculated with statistical methods for a large population of women. The radiation dose absorbed by the glandular tissue in a two-view mammography exam (in terms of Mean Glandular Dose, MGD) is in the order of 2–3 mGy for a standard breast. Such an absorbed dose can be evaluated by means of Monte Carlo calculation of dimensionless coefficients which provide normalized dose values per unit air kerma at the entrance surface of the breast (normalized glandular dose coefficients, DgN) defined for given irradiation geometry, beam quality, breast size and composition. Similarly to mammography, in DBT the MGD is calculated with suitable DgN coefficients, which additionally take into account the irradiation angle of each view and the number and angular position of each projection view.

The present study is meant to investigate the 3D distribution of the average radiation dose affecting the breast tissue, by means of preliminary laboratory experiments in which dosimetric films were positioned at different depths within a layered breast phantom. The purpose was to provide an experimental validation of Monte Carlo calculated dose distributions, also useful for assessment of DgN coefficients in DBT.

2. – Materials and methods

We used a breast phantom (BR3D mod. 020, CIRS Inc., Norfolk, VA, USA) (fig. 1(a)) consisting of 5 slabs, 1-cm thick each, of BR 50/50 material simulating a (50% glandular, 50% adipose) breast, with two components mixed to mimic a heterogeneous

TABLE I. – *Absolute air kerma (ESAK) values (mean ± std. dev.) measured in the ROIs of XR-QA2 radiochromic film exposed free-in-air.*

ROI	$K_{air} \pm \sigma_{Kair}$(mGy)
1	4.6 ± 0.2
2	4.9 ± 0.1
3	4.7 ± 0.1
4	4.6 ± 0.1

adipose/fibroglandular tissue structure. The microfocus X-ray tube (Hamamatsu L8121-03) was operated at 40 kV, 100 μA, 36 mAs, with an added filtration of 1.58 mm Al (fig. 1(b)). The corresponding half value layer was 1.1 mm Al. The distance from the phantom surface to the X-ray focal spot was 56.6 cm, at which the free-in-air air kerma was $K_{\rm air} = (4.57 \pm 0.01)$ mGy (measured with a 20X6-6 ion chamber and a 2026C dosimeter, Radcal Corp., Monrovia, CA, USA). Radiochromic dosimetric films (GAFCHROMIC® films) type XR-QA2 (Ashland Inc., Covington, KY, USA) (lot #01311401, pieces size $11.2 \times 25.3\,\text{cm}^2$ or $12.6 \times 19.2\,\text{cm}^2$) were used for reference dosimetry [4].

The breast phantom was positioned above a series of PMMA slabs simulating the chest wall; a tungsten collimator in front of the X-ray tube window produced a half cone beam, with its base coincident with the phantom base. Film pieces cut from the XR-QA2 sheets were placed at the front surface ($d = 0$ cm), and at $d = 1$ cm, 2 cm, 3 cm, 4 cm, and 5 cm from the surface, sandwiched between adjacent slabs of the BR3D phantom, and they were irradiated at normal incidence ($\theta = 0\,^\circ$) of the central X-ray beam with respect to the entrance surface of the phantom. Then, two additional projections were acquired at $+25\,^\circ$ and $-25\,^\circ$ viewing angles, and pieces of XR-QA2 radiochromic films were positioned at 3-cm depth in the slabs. A film sheet was also exposed free-in-air (*i.e.*, without the phantom in the beam) at 56.6 cm from the source, in order to measure the 2D distribution of the entrance surface air kerma (ESAK) with the calibrated XR-QA2 film.

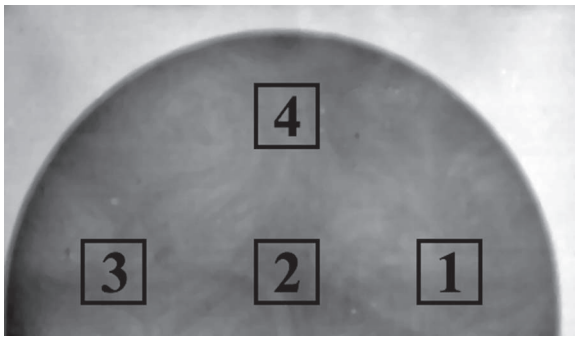

Fig. 2. – Example of a dose map in the CIRS BR3D mod. 020 phantom, obtained by placing a sheet of XR-QA2 radiochromic film at a 2 cm depth in the phantom. The different gray levels in this image indicate different absorption in the various parts of the non-homogeneous phantom. ROIs 1–4 indicate regions where we calculated the average dose and its standard deviation.

TABLE II. – *Absolute dose values, $K^i_{phantom}(d,\theta=0)$, (mean ± std. dev.) measured in the ROIs at depth d in the phantom, where $d=0$ is the front surface of the CIRS BR3D phantom for $\theta = 0^\circ$ viewing angle (cranio-caudal view). The values in parenthesis are $D^i(d,\theta)$ with $K^1_{air} = 4.6\,mGy$.*

d(cm)	ROI 1 $K^1_{phantom} \pm \sigma_{K^1_{phant}}$ (mGy)	ROI 2 $K^2_{phantom} \pm \sigma_{K^2_{phant}}$ (mGy)	ROI 3 $K^3_{phantom} \pm \sigma_{K^3_{phant}}$ (mGy)	ROI 4 $K^4_{phantom} \pm \sigma_{K^4_{phant}}$ (mGy)
0	4.89 ± 0.09	4.94 ± 0.09	4.71 ± 0.08	4.83 ± 0.10
	(1.07 ± 0.05)	(1.08 ± 0.05)	(1.03 ± 0.05)	(1.06 ± 0.05)
1	3.86 ± 0.14	3.62 ± 0.16	3.33 ± 0.10	3.19 ± 0.16
	(0.84 ± 0.05)	(0.79 ± 0.05)	(0.73 ± 0.04)	(0.70 ± 0.05)
2	2.45 ± 0.11	2.22 ± 0.14	2.29 ± 0.11	2.49 ± 0.16
	(0.53 ± 0.03)	(0.49 ± 0.04)	(0.50 ± 0.03)	(0.54 ± 0.04)
3	1.99 ± 0.13	1.86 ± 0.10	1.77 ± 0.11	2.07 ± 0.12
	(0.43 ± 0.03)	(0.41 ± 0.03)	(0.39 ± 0.03)	(0.45 ± 0.03)
4	1.24 ± 0.09	1.18 ± 0.09	1.01 ± 0.10	1.20 ± 0.11
	(0.27 ± 0.02)	(0.26 ± 0.02)	(0.22 ± 0.02)	(0.26 ± 0.03)
5	1.10 ± 0.07	1.31 ± 0.10	1.33 ± 0.11	1.07 ± 0.09
	(0.24 ± 0.02)	(0.29 ± 0.02)	(0.29 ± 0.03)	(0.23 ± 0.02)

Radiochromic films are optically opaque films which develop a blue color upon absorption of ionizing radiation. Hence, a spatially resolved measure of the change in their optical reflectance after irradiation, can be related to the map of absorbed dose. Films were scanned before irradiation with a flatbed scanner (Epson Perfection V750 PRO) and with an image resolution of 72 dots per inch in 48 bit RGB mode and saved as tagged image file format (TIFF) image files. The irradiated films were scanned 24 h post-irradiation using the same protocol as for the un-irradiated films. For the same film piece, the pixel values (PV) were sampled over the same region of interest (ROI) on two images: before and after irradiation. The change in reflectance, ΔR^{i} (difference between reflectance of unexposed and exposed XR-QA2 film pieces), and its standard deviation, $\sigma_{\Delta R^i}$, for the i-th ROI, were evaluated in the red channel of the TIFF image as follows:

$$\Delta R^i = R^i_{before} - R^i_{after} = \frac{1}{2^{16}}[PV^i_{before} - PV^i_{after}], \tag{1}$$

$$\sigma_{\Delta R^i} = \frac{1}{2^{16}}\sqrt{\left(\sigma(PV^i_{before})\right)^2 + \left(\sigma(PV^i_{after})\right)^2}. \tag{2}$$

The calibration curve (free-in-air air kerma *vs.* change in optical reflectance, ΔR, of the film) was linear up to 10 mGy, and was expressed as

$$K_{air} = c \times \Delta R, \tag{3}$$

where c is the film calibration factor. The air kerma provided by the tissue-equivalent calibrated film, when inserted in the phantom, was assumed to be proportional to the average dose in the 50/50 breast phantom material, via a coefficient dependent on the

TABLE III. – *Absolute dose values (mean ± std. dev.) measured in the ROIs at different viewing angles, θ. The values in parenthesis represent absolute dose divided by K_{air} (4.6 mGy).*

	ROI 1	ROI 2	ROI 3	ROI 4
θ (°)	$K^1_{phantom} \pm \sigma_{K^1_{phant}}$ (mGy)	$K^2_{phantom} \pm \sigma_{K^2_{phant}}$ (mGy)	$K^3_{phantom} \pm \sigma_{K^3_{phant}}$ (mGy)	$K^4_{phantom} \pm \sigma_{K^4_{phant}}$ (mGy)
+25	2.14 ± 0.08	2.00 ± 0.07	2.16 ± 0.12	1.94 ± 0.15
	(0.47 ± 0.03)	(0.44 ± 0.03)	(0.47 ± 0.03)	(0.42 ± 0.04)
0	1.99 ± 0.13	1.86 ± 0.10	1.77 ± 0.11	2.07 ± 0.12
	(0.43 ± 0.03)	(0.41 ± 0.03)	(0.39 ± 0.03)	(0.45 ± 0.03)
−25	1.87 ± 0.16	2.00 ± 0.09	2.15 ± 0.11	1.89 ± 0.15
	(0.41 ± 0.04)	(0.44 ± 0.03)	(0.47 ± 0.03)	(0.41 ± 0.04)

beam spectrum, according to the following relation:

$$K^i_{phantom}(d,\theta) = K_{air} \times \left(\frac{\mu_{en}}{\rho}\right)^{phantom}_{air}, \tag{4}$$

where $(\frac{\mu_{en}}{\rho})^{phantom}_{air}$ is the ratio of the mass energy absorption coefficient of the phantom material to that of the air, averaged over the beam spectrum. By dividing the 2D dose

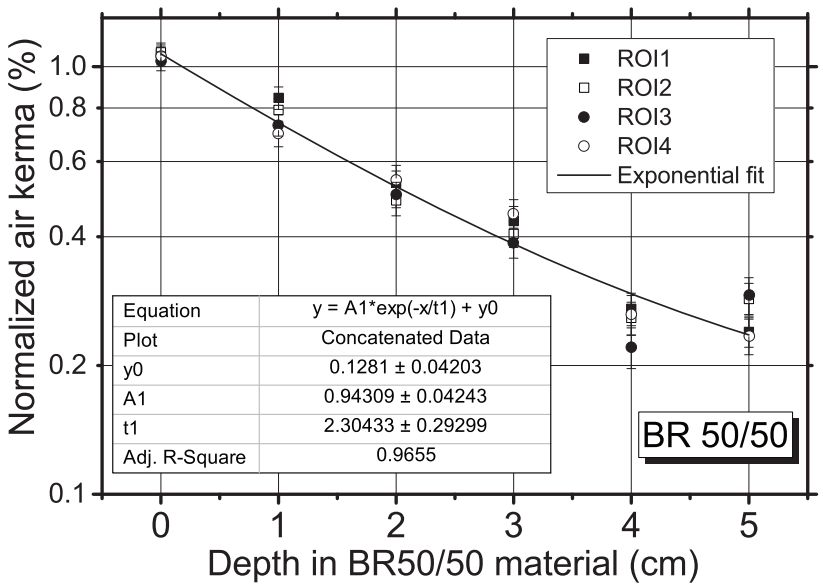

Fig. 3. – Normalized air kerma, $D^i(d, \theta = 0)$ as a function of depth in the phantom, measured in the four ROIs shown in fig. 2. Note that the film at $d = 5$ cm depth records the exit dose map at the phantom/air interface, while the film at 0 cm depth measures the entrance dose map at the air/phantom interface. The continuous line is a weighted fit to all data points with the equation $y = A_1 \times \exp(-x/t_1) + y_0$.

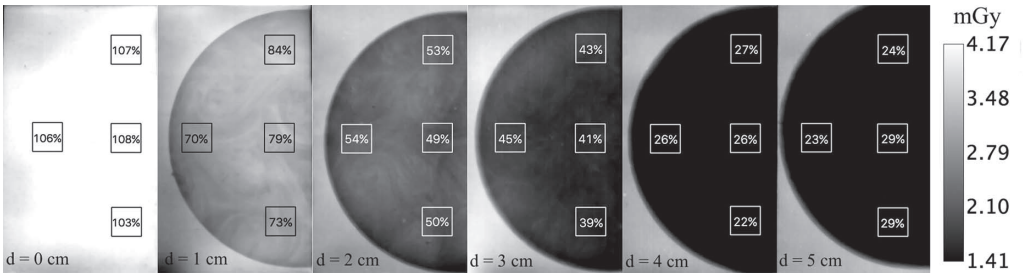

Fig. 4. – Dose maps, $K^i_{phantom}(d, \theta = 0)$, (kerma in BR50/50 in mGy) at various depths, d, in the phantom, for $\theta = 0\,^\circ$ viewing angle (cranio-caudal view). The squares in each map indicate the percentage dose in four ROIs (three at the chest wall and one at the nipple) normalized to $K_{air} = 4.6\,\text{mGy}$. A relative dose higher than 100% indicates the influence of backscatter at the entrance surface.

map at depth d (from $d = 0$ to $d = 5\,\text{cm}$) and at different viewing angles, θ ($\pm 25\,^\circ$), by the ESAK dose map, we obtained the map of normalized dose, D^i, (in terms of air kerma) as a function of depth in the breast phantom and as a function of the viewing angle, according to the following formula:

$$D^i(d, \theta) = \frac{K^i_{phantom}(d, \theta)}{K^1_{air}}, \tag{5}$$

where K^1_{air} is the air kerma measured in the specific region of interest (ROI), ROI 1 (see below), of the film sheet exposed free-in-air.

Finally, we calculated the variation of normalized dose at depth, that is the difference between the normalized dose in each couple of ROI at all depths, d, and all viewing angle, θ, according to the following formula:

$$D^{(i,j)}_{\%}(d, \theta) = |D^i(d, \theta) - D^j(d, \theta)| \times 100, \tag{6}$$

where $D^i(d, \theta)$ is the normalized dose in the i-th ROI, and $D^j(d, \theta)$ is the normalized dose in the j-th ROI.

Moreover, when the beam direction is changed to $\pm 25\,^\circ$, the variation of the normalized dose in the plane at $d = 3\,\text{cm}$ depth in the phantom, $D^{(i,\theta)}_{\%}(3, \theta)$, is calculated as the difference between the normalized dose in the i-th ROI at $\theta = 0\,^\circ$, $D^{(i,0)}(3, \theta)$, and the normalized dose in the i-th ROI at $\theta = \pm 25\,^\circ$, $D^{(i,\theta)}(3, \theta)$, according to the following formula:

$$D^{(i,\theta)}_{\%}(3, \theta) = |D^{(i,0)}(3, \theta) - D^{(i,\theta)}(3, \theta)| \times 100. \tag{7}$$

3. – Results

To investigate the volume dose distribution, we selected four equal-area ROIs: three at the side of the chest wall (ROIs 1–3) and one at the nipple (ROI 4) (fig. 2). Table I shows the average and the standard deviation of $K^i_{phantom}(d, \theta)$ and, in parentheses, the normalized doses, $D^i(d, \theta)$, measured with the radiochromic films in these ROIs. The free-in-air air kerma, K^1_{air}, chosen as reference, was 4.6 mGy (average value evaluated in

TABLE IV. – *Variation of normalized dose, $D^{ij}_{\%}(d,\theta=0)$, at all depths for $\theta = 0\,^\circ$ viewing angle (cranio-caudal view).*

d(cm)	$D^{12}_{\%}(d,0)$ (%)	$D^{13}_{\%}(d,0)$ (%)	$D^{14}_{\%}(d,0)$ (%)	$D^{23}_{\%}(d,0)$ (%)	$D^{24}_{\%}(d,0)$ (%)	$D^{34}_{\%}(d,0)$ (%)
0	1.1	3.8	1.2	5.0	2.3	2.7
1	5.3	11.6	14.8	6.2	9.5	3.2
2	4.8	3.3	0.9	1.5	5.7	4.2
3	2.9	4.9	1.8	2.0	4.7	6.7
4	1.3	5.1	0.8	3.8	0.5	4.2
5	4.6	5.2	0.5	0.6	5.2	5.8

ROI 1). The mean and the standard deviation of normalized doses measured in these ROIs of XR-QA2 films at different depths were reported in table II, and plotted in fig. 3. The percentage dose maps are shown in fig. 4. Irradiation was in cranio-caudal direction ($0\,^\circ$). Figure 5 shows the histogram of dose values at a single depth as well as the combined histogram of dose values at all depths in the phantom, clearly showing the decrease of dose from the entrance to the exit surface.

The average and the standard deviation of normalized doses measured in these ROIs at different viewing angles, θ, were reported in table III, plotted in fig. 6 and the dose percentage change is indicated in fig. 6. Pieces of XR-QA2 radiochromic films were at a 3 cm depth in the phantom (*i.e.*, sandwiched between slab 3 and slab 4 of the 5 cm thick phantom). Table IV shows the values of $D^{ij}_{\%}(d,\theta)$ calculated at all depths. The maximum at each depth goes from 5.0% ($d = 0$ cm) to 14.8% ($d = 1$ cm). Table V shows

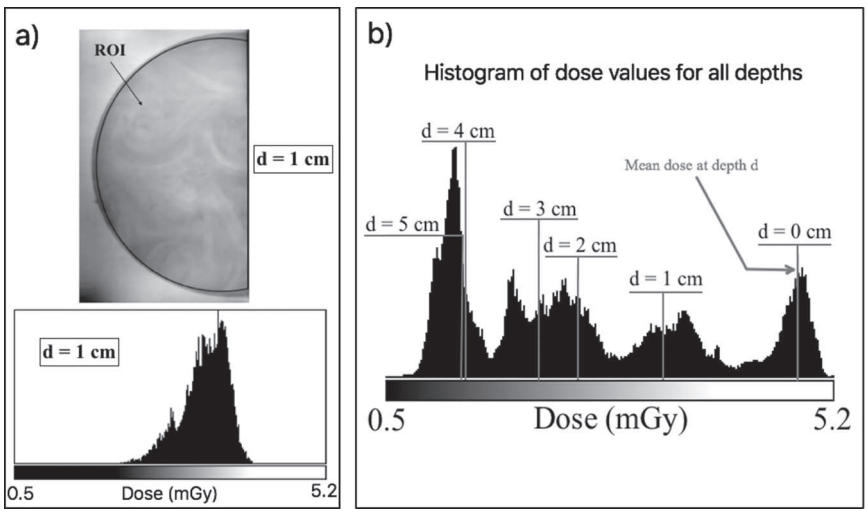

Fig. 5. – (a) Dose histogram (bottom plot) evaluated in a semi-circular ROI covering essentially the whole phantom footprint for the dose map (upper plot) at $d = 1$ cm below the phantom surface. (b) Histogram of dose values evaluated for the dose maps at all six depths in the phantom. Vertical bars indicate the mean dose evaluated across the ROI 2 at the six depths.

TABLE V. – *Variation of normalized dose, $D^{ij}_{\%}(3,\theta)$, at all viewing angles, θ, and at depth $d = 3$ cm.*

$\theta(^\circ)$	$D^{12}_{\%}(3,\theta)$ (%)	$D^{13}_{\%}(3,\theta)$ (%)	$D^{14}_{\%}(3,\theta)$ (%)	$D^{23}_{\%}(3,\theta)$ (%)	$D^{24}_{\%}(3,\theta)$ (%)	$D^{34}_{\%}(3,\theta)$ (%)
+25	3.2	0.4	4.5	3.6	1.3	4.9
0	2.9	4.9	1.8	2.0	4.7	6.7
−25	2.8	6.0	0.5	3.3	2.2	5.5

the values of $D^{ij}_{\%}(3,\theta)$, showing that the maximum variation is 6.7% at 0°. Table VI shows that the maximum variations of $D^{ij}_{\%}(3,\theta)$ (8.6% and 8.3%) occur when the tube is rotated from 0° to +25° or −25°.

The normalized dose in ROI 2 in the phantom decreased from 1.08 (value at the entrance surface of the phantom) to 0.29 at the exit surface of the 5 cm thick phantom, which represents a 71% decrease with respect to the free-in-air entrance air kerma; similar trends were observed for the other ROIs. As noted, for normal beam incidence the maximum variation of the normalized dose for any given plane at depth d goes from 5.0% to 14.8% (table IV); moreover, for any given angle the maximum variation in the plane at a 3 cm depth in the phantom is +6.7% (table V).

When the beam direction was changed to ±25 °, there was a variation of the normalized dose from 2.6% in ROI 1 to 8.6% in ROI 3 (*i.e.*, higher dose in the tilted view than at 0 ° view) (table VI). The backscatter fraction was between 3% and 8%.

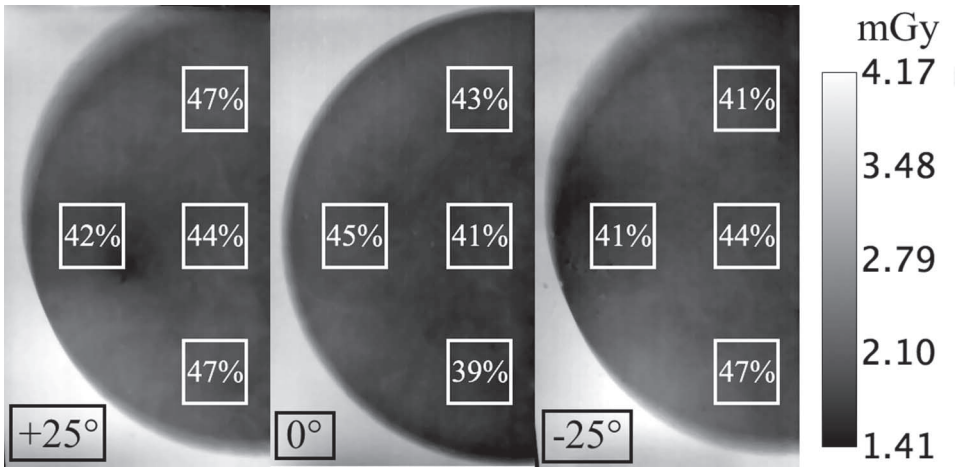

Fig. 6. – Dose maps, $K^i_{phantom}$, measured with the radiochromic film placed at a 3 cm depth in the CIRS BR3D phantom, for viewing angles of +25 °, 0 °, −25 °. The numbers in white color in the squares in each map indicate the percentage of dose in four ROIs normalized to K = 4.6 mGy (*i.e.*, 44% indicates an average absorbed dose in the ROI of 0.44 × 4.6 mGy = 2.02 mGy).

TABLE VI. – *Variation of normalized dose,* $D_{\%}^{(i,\theta)}(3,\theta)$*, in the plane* $d = 3\,cm$ *for angles* $\theta = \pm 25\,^\circ$.

$\theta(\,^\circ)$	$D_{\%}^{(1,\theta)}(3,\theta)$ (%)	$D_{\%}^{(2,\theta)}(3,\theta)$ (%)	$D_{\%}^{(3,\theta)}(3,\theta)$ (%)	$D_{\%}^{(4,\theta)}(3,\theta)$ (%)
+25	3.3	3.1	8.6	3.0
−25	2.6	3.0	8.3	3.9

4. – Discussion

The present work provided preliminary experimental indications of volume dose distribution in a DBT scan, using radiochromic films and a breast phantom. The films were calibrated in terms of free-in-air air kerma, then converted into dose in the breast phantom material. The relative total uncertainty observed for dose values was between 2% and 4%. Significant variations in dose values were observed at depth, in each plane transverse to the beam direction, as well for large tilting of the X-ray beam axis. A new investigation has been carried out and was recently reported [5], confirming and extending the present results.

5. – Conclusions

We successfully measured the volume dose distribution in a layered breast phantom in laboratory tests simulating a digital breast tomosynthesis scan. Dose maps were derived on several planes transverse to the beam axis using radiochromic films, so providing the dose distribution from the entrance to the exit surface and from the chest wall to the nipple. In transverse planes the dose varies up to 14.8% at 0 ° (normal incidence) and up to 8.6% when the X-ray tube is tilted by 25 °. From the entrance to the exit surface, the dose decreases by about 71%. The backscatter fraction is up to 8%. We plan to provide further confirmations of these preliminary findings via measurements with a wider range of irradiation parameters, via measurements of volume dose distribution at all depths (0 cm, 1 cm, 2 cm, 4 cm, 5 cm) when the X-ray tube is tilted by 25 °, and via comparison of dose distributions calculated with a Monte Carlo simulation.

* * *

I am grateful to Prof. Paolo Russo for suggestions and discussions during the preparation of this manuscript. I am also grateful to Dr. Francesca Di Lillo, Dr. Antonio Sarno and Prof. Giovanni Mettivier for their kind help.

REFERENCES

[1] http://www.airc.it/tumori/tumore-al-seno.asp
[2] SECHOPOULOS I., *Med. Phys.*, **40** (2013) 014301.
[3] MALDERA A. *et al.*, *Med. Phys.*, **33** (2017) 56.
[4] TOMIC N. *et al.*, *Med. Phys.*, **37** (2010) 1083.
[5] SARNO A. *et al.*, *IEEE Trans. Rad. Plasma Med. Sci.*, **1** (2017) 322.